MATHEMATICAL REMOVAL OF POSITRON RANGE BLURRING IN HIGH RESOLUTION TOMOGRAPHY*

Stephen E. Derenzo
Donner Laboratory and Lawrence Berkeley Laboratory
University of California
Berkeley, CA 94720

Abstract

Positron range blurring can be removed from PET projection data by Fourier deconvolution. The method uses previously measured positron range spread functions whose 'cusp-like' shape retains some of the higher spatial frequency information. Although the deconvolution process amplifies the statistical noise, especially for for narrow projection bins and for isotopes with high positron energy, it can significantly improve the ability to estimate the amount of positron activity in each region of quantitation.

1. Introduction

Positron Emission Tomography is being used increasingly for the determination of flow and metabolic rate constants in well-defined regions. However, many factors can blurr the reconstructed activity distribution from one region to another. Among these are detector resolution, β^+ range, deviations from 180° emission, off-axis penetration, limited linear or angular sampling, Compton scatter in the detectors, and organ motion.[1] Recent advances in detector resolution [2-11] have made it important to examine the other factors.

In this paper, we investigate the possibility of mathematically removing the blurring caused by β^+ range. It is the goal of this process to nearly eliminate the systematic errors caused by the blurring, although the statistical uncertainty in the projection measurements will be increased.

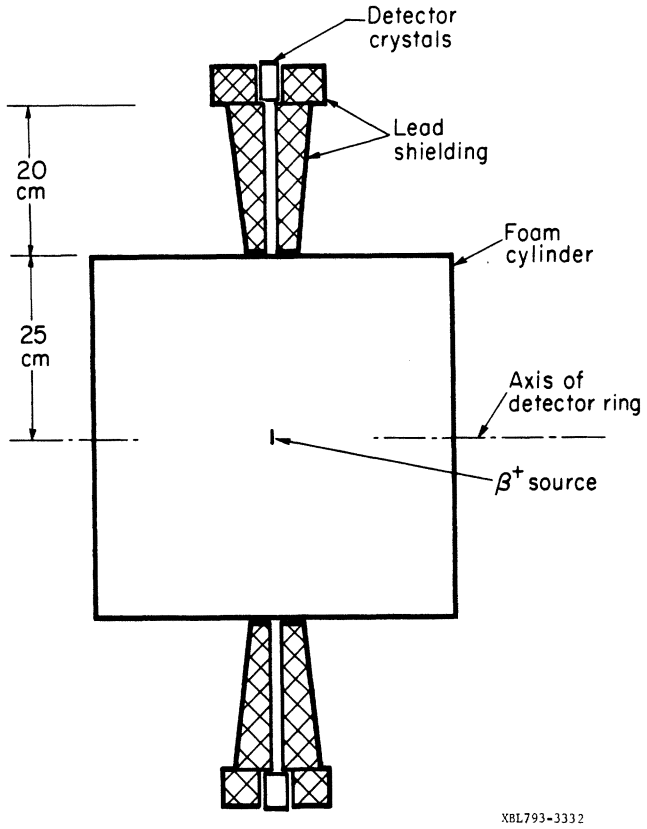

Figure 1: Placement of positron source, polyurethane foam, lead shielding, and detectors for the measurement of the projected positron range point spread function (PSF).

2. Previous Measurements of Positron Range Distributions

In previous work, we measured the positron range distributions for ^{18}F, ^{11}C, ^{68}Ga, and ^{82}Rb sources.[12] The sources were deposited on thin mylar foils, surrounded by polyurethane foam, and placed in the Donner 280-Crystal Positron Tomograph[13] (Fig 1). Parallel ray projection data were measured in 5 mm bins with a resolution of 8 mm FWHM (Full-Width at Half-Maximum). The foam density was 0.02 gm cm^{-3} for ^{18}F, ^{11}C and ^{68}Ga, and 0.05 gm cm^{-3} for ^{82}Rb, and the corresponding resolutions were 0.16 mm and 0.4 mm FWHM water equivalent. The same sources were also surrounded by aluminum to measure all broadening effects other than positron range, such as source size, detector size, deviations from 180° emission, and scattering in the foam or aluminum and lead shielding.

For each isotope, the aluminum projection data were convolved with an empirical positron range function $q(z)$:

$$q(z) = A \cdot EXP(-z/B) + (1 - A) \cdot EXP(-z/C) \quad (1)$$

The three parameters A, B, and C were varied to give the best fit to the foam projection data (Table 1). In all cases, the fit was excellent.[12] The analytical expression for $q(z)$ thus describes only broadening due to positron range (Fig 2).

*This work was supported in part by the Director, Office of Energy Research, Office of Health and Environmental Research of the U.S. Department of Energy, under Contract No. DE-AC03-76SF00098, and in part by the National Institutes of Health, National Heart, Lung, and Blood Institute under grant No. P01 HL25840.

TABLE 1: MEASURED PROJECTED POSITRON RANGE DISTRIBUTIONS

ISOTOPE	^{18}F	^{11}C	^{68}Ga	^{82}Rb
Maximum β^+ Energy (MeV)	0.64	0.96	1.90	3.35
Best fit parameters of equation 1 (see text)				
A	0.851	0.905	0.808	0.873
B (mm)	0.054	0.058	0.166	0.222
C (mm)	0.254	0.440	1.15	2.55
Projected Point Spread Functions:				
FWHM (mm)	0.13	0.13	0.31	0.42
FW(0.1)M (mm)	0.38	0.39	1.6	1.9
rms (mm)	0.23	0.39	1.2	2.6
Projected Line Spread Functions:				
FWHM (mm)	0.22	0.28	1.35	2.6
FW(0.1)M (mm)	1.09	1.86	5.92	13.2
rms (mm)	0.38	0.69	1.60	3.8

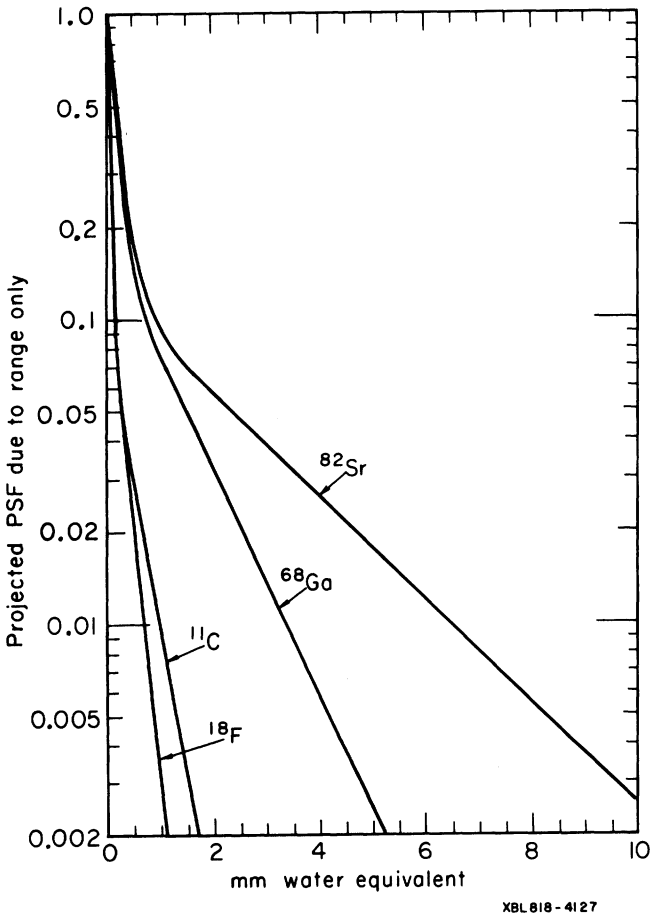

Figure 2: Best fit q(z) positron range projected point spread function (PSF) for the four isotopes, showing the effect of positron range only.

The LSF for each isotope was determined by integration:

$$S(z) = \int q(z')dx, \qquad where\ z' = \sqrt{x^2 + z^2} \tag{2}$$

The projected line spread function is the projection of a line source of activity oriented along the axis of the tomograph (Fig 3).

The positrons are emitted with a range of energies from zero to a maximum which varies from 640 keV for ^{18}F to 3350 for ^{82}Rb. Due to the non-linear relationship between energy and range for sub-relativistic charged particles (such as positrons between 200 keV), a significant fraction of the emitted positrons travel less than 1 mm. The resulting distribution has a central spike that preserves some of the high spatial frequency information. In contrast, the Gaussian distribution that results from deviations from 180° emission is flat at its center and very poorly preserves the higher spatial frequencies.

The positron range distributions have also been measured by Cho et al[14] and by Hoffman et al[15].

3. Generation of Simulated Data

In this work we generated test projection data T in 150 projection bins 2 mm wide covering 300 mm. The test pattern consisted of three sets of hot spots on a 200 mm wide background (Fig 4). The first group has 5 hot spots 4 mm wide with 4 mm wide cold spots between them. The second group has 4 hot spots 6 mm wide with 6 mm wide cold spots. The third group has 3 hot spots 8 mm wide with 8 mm wide cold spots.

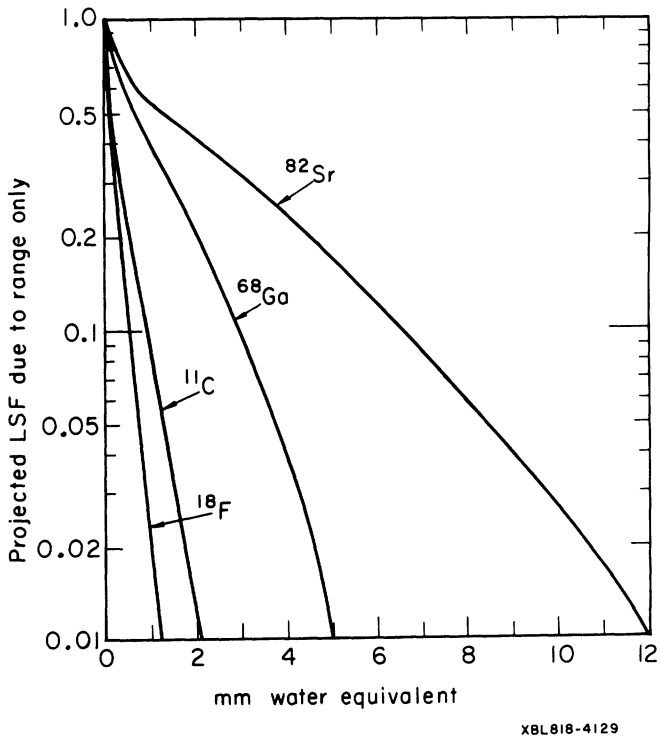

Figure 3: Line spread functions (LSF), computed from the PSFs of Fig 2.

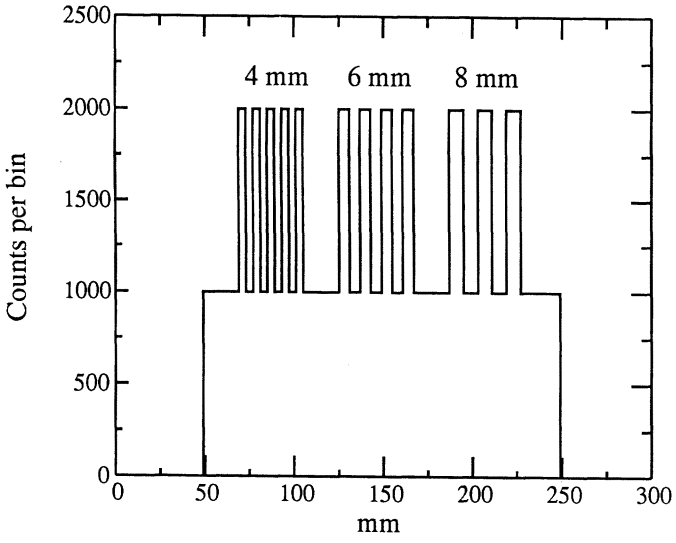

Figure 4: Test projection data in 2 mm wide projection bins of three groups of hot spots (1000 events per bin) added to a 200 mm wide background (1000 events per bin). The first group has 5 hot spots 4 mm wide with 4 mm wide cold spots between them. The second group has 4 hot spots 6 mm wide with 6 mm wide cold spots. The third group has 3 hot spots 8 mm wide with 8 mm wide cold spots.

The projected line spread functions (Fig. 3) were integrated over each bin to produce the distribution R, which was convolved with the test projection data T to produce the distribution $S = T \otimes R$.

$$S_i = \sum_j T_{j-i} \cdot R_j \tag{3}$$

Gaussian noise was then added (Fig 5A):

$$S_i' = S_i + \sum_{k=1}^{12} Q_k \sqrt{S_i} \tag{4}$$

where Q_k is a random variable, uniformly distributed between -0.5 and +0.5. This added noise had a mean of zero and a variance equal to the number of events per bin S_i. The projection bin data were treated as independent measurements.

4. Procedure for Deconvolving Positron Range

To deconvolve the positron range blurring for each isotope, the 1-dimensional discrete Fourier transform of the arrays S' and R were computed.[16] The deconvolved projection array T' was computed as the inverse Fourier transform of the quotient (Fig 5B):

$$T' = \mathcal{F}^{-1}[\mathcal{F}(S')/\mathcal{F}(R)] \tag{5}$$

Because the positron range distribution has a significant fraction of annihilations in the central 1 mm bin, the deconvolution process is able to recover frequencies on the order of 0.5 cycle per mm, but only by amplifying the noise component at these higher frequencies. The result is an increase in the statistical uncertainty, as shown in Table 2 and Fig 6. The increase is less for emitters that have lower positron energy, and less for wider projection bins, because the positron range distribution best preserves the lower spatial frequencies.

Note that the most commonly used reconstruction algorithms work by first filtering the projection data to deconvolve the function 1/R, and then backprojecting. By modifying the filter (a multiplication in Fourier space), the positron range can be deconvolved during the reconstruction with no additional computational effort.

Equivalently, the projection data S' can be convolved with a function K, called the range deconvolution kernel:

$$T' = K \otimes S' \quad K = \mathcal{F}^{-1}[\mathcal{F}(R)]^{-1} \tag{6}$$

The square of the increase in rms statistical error (the variance amplification) (Fig 6) may be computed as the sum of the squares of the elements of K.

$$[E'/E_{stat}]^2 = \sum K_i^2 \tag{7}$$

5. Interpretation of Results

The blurring due to positron range can cause a significant distortion in the initial distribution T. To describe the effect of range blurring only, we define a Systematic rms deviation between the initial projection data T and the burred projection data S:

$$E_{sys} = \sqrt{\frac{1}{n}\sum_{i=1}^{n}\left[\frac{(S_i - T_i)}{T_i}\right]^2} \tag{8}$$

The addition of Gaussian noise further degrades the data, and this can be described by the familiar statistical rms deviation between the blurred projection data S and the blurred, noisy projection data S':

$$E_{stat} = \sqrt{\frac{1}{n}\sum_{i=1}^{n}\left[\frac{(S_i' - S_i)}{S_i}\right]^2} \tag{9}$$

Together, the difference between the S' and the initial distribution T can be described as a combined rms deviation between the initial projection data T and the blurred, noisy projection data S':

$$E = \sqrt{\frac{1}{n}\sum_{i=1}^{n}\left[\frac{(S_i' - T_i)}{T_i}\right]^2} \tag{10}$$

After the deconvolution process described in Equation 5, the systematic error is very small but the statistical error has been increased, as described by the rms deviation between the initial projection data T and the deconvolved projection data T':

$$E' = \sqrt{\frac{1}{n}\sum_{i=1}^{n}\left[\frac{(T_i' - T_i)}{T_i}\right]^2} \tag{11}$$

As seen in Table 2, by reducing the systematic error, the mathematical deconvolution of positron range can reduce the rms deviations between the initial and deconvolved distributions, even though the statistical component is increased. For example in the case of ^{68}Ga, 2 mm bins, and the projection data of Fig. 4, the positron range blurring causes an rms deviation from the initial data of 14.5%, which is increased to 14.9% by the addition of Gaussian noise. The deconvolution procedure reduces this rms deviation to 8.1% due to the decrease in systematic error, even though the statistical errors have been increased in the process. It will be the subject of future work to determine the effect of this procedure on reconstructed images as a function of bin width, isotope, and number of events.

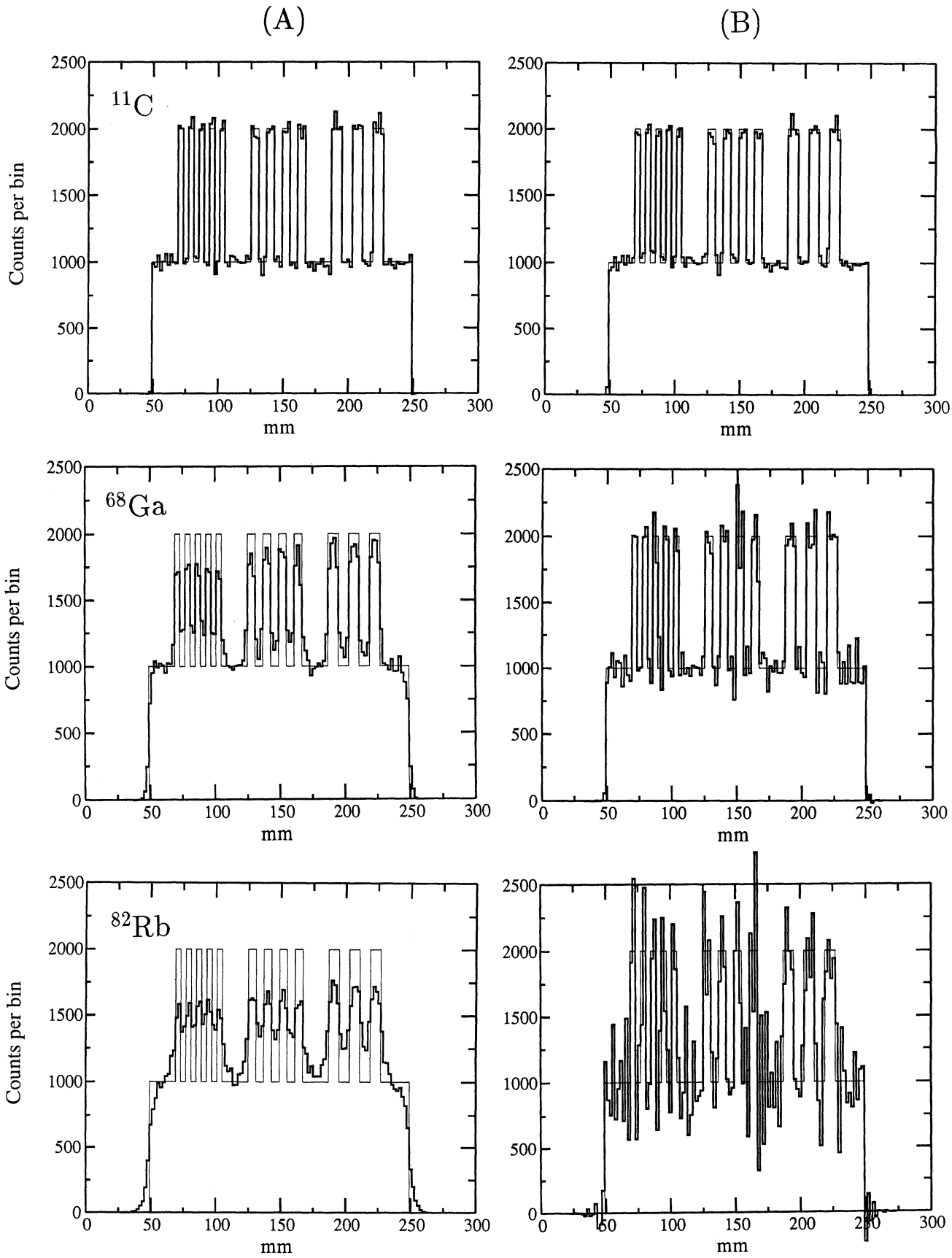

Figure 5:
(A) Test data of Fig 4 convolved with the LSFs for ^{11}C, ^{68}Ga, and ^{82}Rb (Fig 3) and added to Gaussian noise with mean = zero and variance = number of events per bin. Light lines show original data.
(B) Data from B after deconvolution of the positron range LSFs.

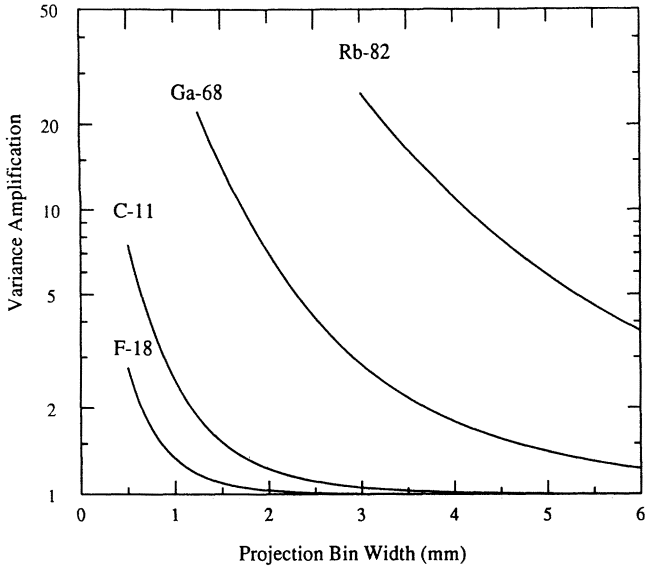

Figure 6: Plot of the variance amplification (7) that results from the positron range deconvolution process

TABLE 2: CHANGE IN SYSTEMATIC AND STATISTICAL ERRORS DUE TO THE FOURIER DECONVOLUTION OF POSITRON RANGE[a]

Isotope	W (mm)[b]	E_{sys} (Eqn 8)	E_{stat} (Eqn 9)	E (Eqn 10)	E' (Eqn 11)
^{18}F	1	2.4%	2.9%	4.0%	3.3%
	2	0.4%	2.4%	2.5%	2.5%
^{11}C	1	6.0%	2.7%	6.7%	4.4%
	2	2.6%	3.0%	4.1%	3.3%
^{68}Ga	1	16.1%	3.2%	16.5%	20.0%
	2	14.5%	2.8%	14.9%	8.1%
^{82}Rb	1	25.3%	2.7%	25.8%	47.2%
	2	24.8%	2.6%	25.0%	22.5%

[a] For the projection data of Fig. 4
[b] Projection bin width, usually one-half of the geometrical spatial resolution FWHM.

6. Conclusions

(1) Positron range blurring can be mathematically removed from PET projection data by Fourier deconvolution.

(2) The deconvolution process amplifies the noise, and this effect is greatest for narrow projection bins and for positron isotopes with large maximum positron energy.

(3) The method significantly reduces systematic errors due to positron range blurring, and improves the quantitative accuracy of the amount of positron activity in each projection bin.

(4) This method will be most effective for ^{11}C data at resolutions from 2 to 5 mm FWHM and for ^{82}Rb data at resolutions from 5 to 15 mm FWHM. It does not appear as important to deconvolve the positron range blurring from ^{18}F and ^{11}C data, because it is less than other factors such as deviations from 180° emission.

Acknowledgements

I Thank R. Huesman, B. Mazoyer, and T. Budinger for helpful discussions.

This work was supported in part by the Director, Office of Energy Research, Office of Health and Environmental Research of the U.S. Department of Energy, under Contract No. DE-AC03-76SF00098, and in part by the National Institutes of Health, National Heart, Lung, and Blood Institute under grant No. P01 HL25840.

References

1. Derenzo SE, Budinger TF, and Huesman RH: Detectors for high resolution dynamic PET. In *The Metabolism of the Human Brain Studied with Positron Emission Tomography,* T. Greitz and D. Ingvar, Eds, Raven Press, New York, pp 21-31, 1985
2. Burnham CA, Bradshaw J, Kaufman D, et al: A stationary positron emission ring tomograph using BGO detector and analog readout. *IEEE Trans Nucl Sci* **NS-31:** 632-636, 1984
3. Brownell GL, Burnham CA and Chesler DA: High resolution tomograph using analog coding. In *The Metabolism of the Human Brain Studied with Positron Emission Tomography,* Greitz T and D. Ingvar, eds, Raven Press, New York, 1985, pp 13-20
4. Stearns CW, Chesler DA, Kirsch JE, et al: Quantitative imaging with the MGH analog ring positron tomograph. *IEEE Trans Nucl Sci* **NS-32:** 898-901, 1985
5. Burnham CA, Bradshaw J, Kaufman D, et al: Design of cylindrical shaped scintillation camera for positron tomographs. *IEEE Trans Nucl Sci* **NS-32:** 889-893, 1985
6. Nohara N, Tanaka E, and Tomitani T: Analytical study of performance of high resolution positron emission computed tomographs for animal study. *IEEE Trans Nucl Sci* **NS-32:** 818-821, 1985
7. Tomitani T, Nohara N, Morayama H, et al: Development of a high resolution positron CT for animal studies. *IEEE Trans Nucl Sci* **NS-32:** 822-825, 1985
8. Computer Technology and Imaging, Inc. Knoxville, Tennessee, MODEL PT 931 ECAT Scanner System Description.
9. Derenzo SE, Huesman RH, Budinger FT, Cahoon JL, and Vuletich T: High resolution positron emission tomography using 3 mm wide bismuth germanate crystals, 1985 (in preparation)
10. Karp JS and Muehllehner G: Performance of a position-sensitive scintillation detector. *Phys Med Biol* 1985 (in press)
11. Muehllehner G and Karp JS: A positron camera using position sensitive detectors: PENN–PET. (submitted for publication) 1985
12. Derenzo, SE: Precision measurement of annihilation point spread distributions for medically important positron emitters. In: *Positron Annihilation,* Hasiguti RR and Fujiwara K, eds, pp 819-823, The Japan Institute of Metals, Sendai, Japan, 1979
13. Derenzo SE, Budinger TF, Huesman, RH, Cahoon JL and Vuletich T: Imaging properties of a positron tomograph with 280 BGO crystals. *IEEE Trans Nucl Sci* **NS-28:** 81-89, 1981
14. Cho ZH, Chan JK, Eriksson L, et al: Positron ranges obtained from biomedically important positron-emitting radionuclides. *J Nucl Med* **16:** 1174-1176, 1975
15. Hoffman EJ, Phelps ME, Mullani NA, et al: Design and performance characteristics of a whole-body positron transaxial tomograph. *J Nucl Med* 17: 493-502, 1976
16. Brigham E. Oran: *The Fast Fourier Transform,* Prentice-Hall, Inc., Englewood Cliffs, N.J., 1974